PROCEEDINGS OF SCIENCE

Updated Analysis of SuperTIGER Flight Data for Galactic Cosmic-Ray Elemental Spectra

A.W. Labrador[a,*], Q. Abarr[b], Y. Akaike[c], W.R. Binns[b], R.G. Bose[b], T.J. Brandt[c], N. Cannady[c], P. Ghosh[c,d], T. Hams[c,d], M.H. Israel[b], L. Lisalda[b], R.A. Mewaldt[a], J.W. Mitchell[c], R.P. Murphy[b], S. Nutter[e], N. Osborne[b], B.F. Rauch[b], K. Sakai[c,d], M. Sasaki[c,d], E.C. Stone[a], C.J. Waddington[f], N.E. Walsh[b], J.E. Ward[b], A. West[b], M.E. Wiedenbeck[g], and W. Zober[b]

[a] *California Institute of Technology, Pasadena, CA 91125 USA*
[b] *Washington University, St. Louis, MO 63130 USA*
[c] *NASA/Goddard Space Flight Center, Greenbelt, MD 20771 USA*
[d] *Center for Research and Exploration in Space Science and Technology (CRESST), Greenbelt, MD 20771, USA*
[e] *Northern Kentucky University, Highland Heights, KY USA*
[f] *The University of Minnesota, Minneapolis, MN 55455, USA*
[g] *Jet Propulsion Laboratory, California Institute of Technology, Pasadena, CA 91109 USA*
[*] *E-mail: labrador@srl.caltech.edu*

SuperTIGER (Trans-Iron Galactic Element Recorder) is a large-area, balloon-borne cosmic-ray experiment designed to measure the galactic cosmic-ray abundances of elements from Z=10 (Ne) to Z=56 (Ba) at energies from ~0.8 GeV/nuc to ~10 GeV/nuc, with the primary goal of measuring relative abundances of ultra-heavy elements above Z=30. SuperTIGER flew for a record 55 days over Antarctica in 2012-2013 and for a second flight of over 32 days in 2019-2020. Although the primary goal is measuring ultra-heavy cosmic-ray relative abundances, the SuperTIGER data analysis uses measurements of abundant elements at Z<30 for precise charge calibration extended to the ultra-heavy elements. In this technical presentation, we will report ongoing progress on analysis to obtain energy spectra for these Z<30 elements, from Ne to Cu. We will present new details of the aerogel and acrylic Cherenkov calibrations necessary for calculating energies for generating absolute spectra, including effective photoelectron resolution, knock-on electron contributions, and other background signals in the Cherenkov detectors.

38th International Cosmic Ray Conference (ICRC2023)
26 July - 3 August, 2023
Nagoya, Japan

[*] Speaker

PoS(ICRC2023)128

1. Introduction

SuperTIGER (Trans-Iron Galactic Element Recorder) is a large area, balloon-borne experiment designed and flown to measure the galactic cosmic-ray abundances of elements from Ne (Z=10) to Ba (Z=56) at ~0.8–10 GeV/nuc. SuperTIGER had a record-breaking flight of 55 days around Antarctica, from December 8, 2012 to February 1, 2013 [1] and another, shorter flight from December 16, 2019 to January 16, 2020.

Previously reported relative abundances of ultraheavy elements ($30 \leq Z \leq 40$) in SuperTIGER 2012-2013 data are consistent with galactic cosmic ray origins in OB associations with preferential acceleration of refractory elements over volatile elements [2]. Additionally, relative abundances of iron secondaries measured by SuperTIGER, e.g. (Sc+Ti+V)/Fe, are consistent with HEAO measurements as well as Standard Leaky Box Model calculations [3,4].

While these results make use of measured element ratios in SuperTIGER data, we have abundant data at Z=11–29 to attempt to determine absolute spectral intensities. Previous work included attempts to detect microquasar signatures in $_{26}$Fe spectra, but those spectra were scaled to match ACE/CRIS spectra at lower energies [3]. In order to obtain absolute intensities, corrections for energy losses and interactions in both the instrument and atmosphere must be undertaken with the help of detailed Geant4 simulations of the instrument. This work was initiated in 2019 [5], and this paper describes significant extensions of that work.

2. The SuperTIGER Geant4 Model

The SuperTIGER instrument is described in detail by Binns et al. [1]. The payload is divided into two nearly identical modules. Each module is composed of a stack of several detectors. The detectors in each module are a plastic scintillator (S1) for charge measurement, a scintillating optical fiber hodoscope system (H1 at top, and H2 at bottom) to measure particle trajectories, an aerogel Cherenkov detector (C0) (refractive index n=1.025 or n=1.043) to measure charge and velocity, an acrylic Cherenkov (n=1.49) detector (C1) also for charge and velocity, another plastic scintillator (S2) above H2, and a third plastic scintillator (S3) below. In one module, the aerogel blocks in the C0 detector are entirely n=1.043 refractive index aerogels (threshold energy of ~2.5 GeV/nuc), while in the other module, half of the C0 aerogels have a refractive index n=1.043 while the other half have n=1.025 (threshold energy ~3.3 GeV/nuc). Particle data are stored in onboard solid state drives as well as transmitted via line-of-sight (LOS) telemetry or Tracking and Data Relay Satellite System (TDRSS).

We use the Geant4 library [6] to construct models of the the SuperTIGER instrument and to simulate its responses to incident energetic charged particles. The simulations include a physical description of the payload, specifically the bulk materials in the particle beam. Support structures outside of the particle beam as well as materials with negligible mass are not included (e.g the thin film wrapping the aerogels). Test particles (e.g. $_{26}$Fe) are simulated with normal or isotropic incidence, depending on application, and varying kinetic energies from 200 MeV/nuc to >10 GeV/nuc. Using the default physics models, the Geant4 code simulates ionization energy

losses and energy deposited in all materials, scattering, and production of secondary particles. Figure 2 shows a sample $_{26}$Fe event going through a SuperTIGER model and creating secondary particles. Figure 3 shows models for the two Geant4 modules.

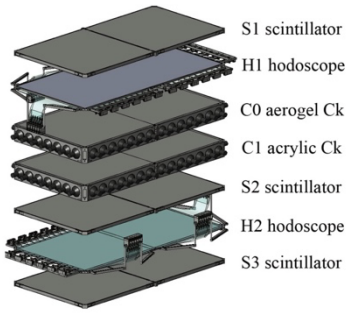

Figure 1: Expanded view of one SuperTIGER module, from Binns et al. [1].

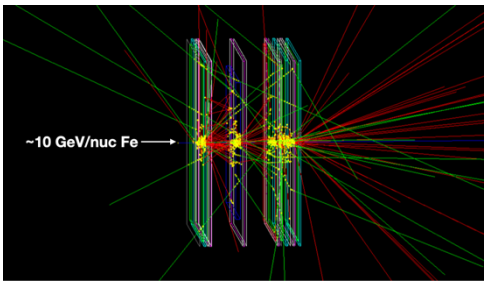

Figure 2: A simulated 10 GeV/nuc 26Fe particle passing through SuperTIGER material.

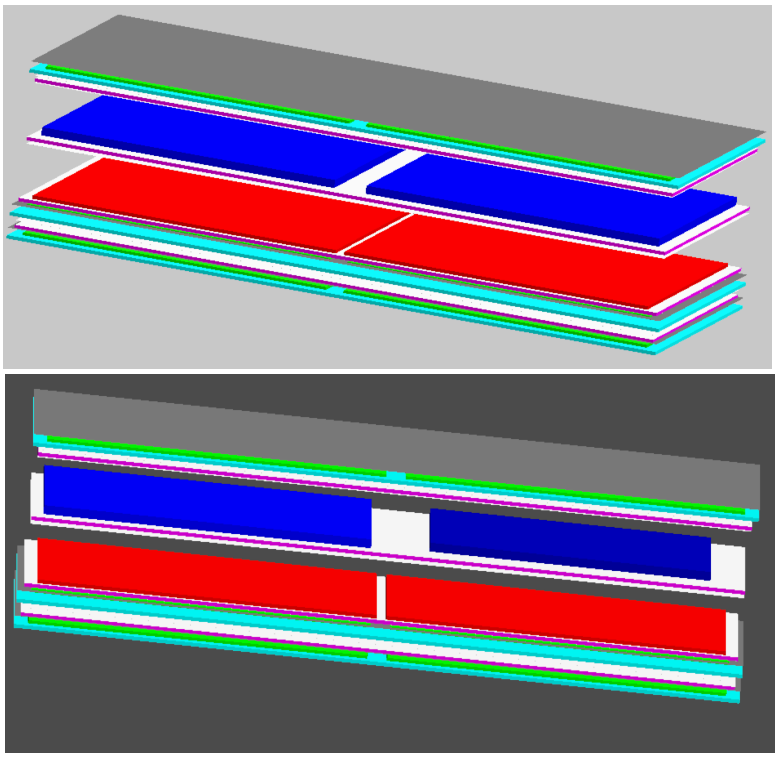

Figure 3: Geant4 models of the SuperTIGER module with two n=1.043 aerogel sections (top; aerogels in dark blue), and the module with one n=1.043 and one n=1.025 aerogel sections (bottom). The n=1.025 aerogels are smaller than the n=1.043 aerogels. These models are used both for the interaction loss and energy shift corrections but also to calculate geometry factor.

3. Interaction Losses

When particles pass through the SuperTIGER detectors, they lose or deposit energy as well as produce secondary particles, and some of those particles are a result of nucleons breaking off the incident nuclei. Since energies deposited in matter are proportional to $\sim Z^2$ for each incident particle, the energies deposited will change significantly in layers after such charge changing interactions. During flight data analysis, particles undergoing interaction losses are eliminated by charge consistency selection criteria, usually imposed between the S1 and S2 scintillators; the addition of S3 has been found to make only a small contribution the overall charge consistency cut [1]. Regardless, the loss of incident particles due to charge consistency cuts must be corrected for in order to obtain elemental abundances at the top of the instrument and the top of the atmosphere.

Figure 4 shows Geant4 calculations (for Z=22 to Z=27) of inelastic interaction losses through the instrument. Each figure shows the fraction of particles incident at the top of the instrument that survive without changing charge to S1, S2, and S3 vs. energy (MeV/nuc). Thus, for ~500 MeV/nuc $_{26}$Fe, about 80% of the particles survive through S1, but only ~50% survive through S2 and ~45% survive through S3. For each of these curves, 200k particles with energies from 200 MeV/nuc to 40 GeV/nuc were simulated in a power law spectrum with an index of -2. Simulations were run for Z=10 through Z=29, and matrices were constructed to tabulate interaction losses through each layer.

4. Energy Losses

Since velocities are calculated from the aerogel and acrylic Cherenkov signals (C0 and C1), the energies derived by those Cherenkov signals have to be corrected to the top of the instrument (TOI) and top of the atmosphere (TOA) for losses in the atmosphere and instrument above each Cherenkov detector. Figure 5 shows Geant4 calculations of relative energies at TOI and at the top of C1, compared to the top of C0, for ~200 MeV/nuc to 10 GeV/nuc $_{26}$Fe. For ~500 MeV/nuc $_{26}$Fe at C0, the same particle would lose almost 5% of its energy before the top of C1 (i.e. hitting ~475 MeV/nuc), while that same particle would have had about 15% more energy at the top of the instrument, or a total energy of 575 MeV/nuc. As shown in Figure 4, at higher energies, the relative differences become negligible.

5. Knock-on Electron Corrections

Just above Cherenkov threshold for a primary incident particle, signals from knock-on electrons (delta-rays) can be comparable in magnitude to the primary particle signal, so corrections to the Cherenkov signals must be obtained and applied to the energy calibrations. Figure 6 shows the result of Geant4 simulations, showing $_{26}$Fe Cherenkov signals for primary particles in red (two bands, for n=1.043 (upper) and n=1.025 (lower) aerogel blocks), knock-on electron signals (blue) primarily due to knock-on electrons

induced by the primary particles above Cherenkov threshold, and knock-on electron signals (green) due to knock-on electrons produced by primaries below Cherenkov threshold.

Above primary threshold energy, the dense band of low knock-on signals are due to knock-on electrons produced primarily within the aerogel Cherenkov radiator, and less-dense scattering of higher knock-on signals are due primarily to other secondaries (e.g. He, in addition to electrons) produced in the overlying material in the detector stack. As charge-changing interactions, these particles are removed from flight data analysis via charge-consistency selection criteria.

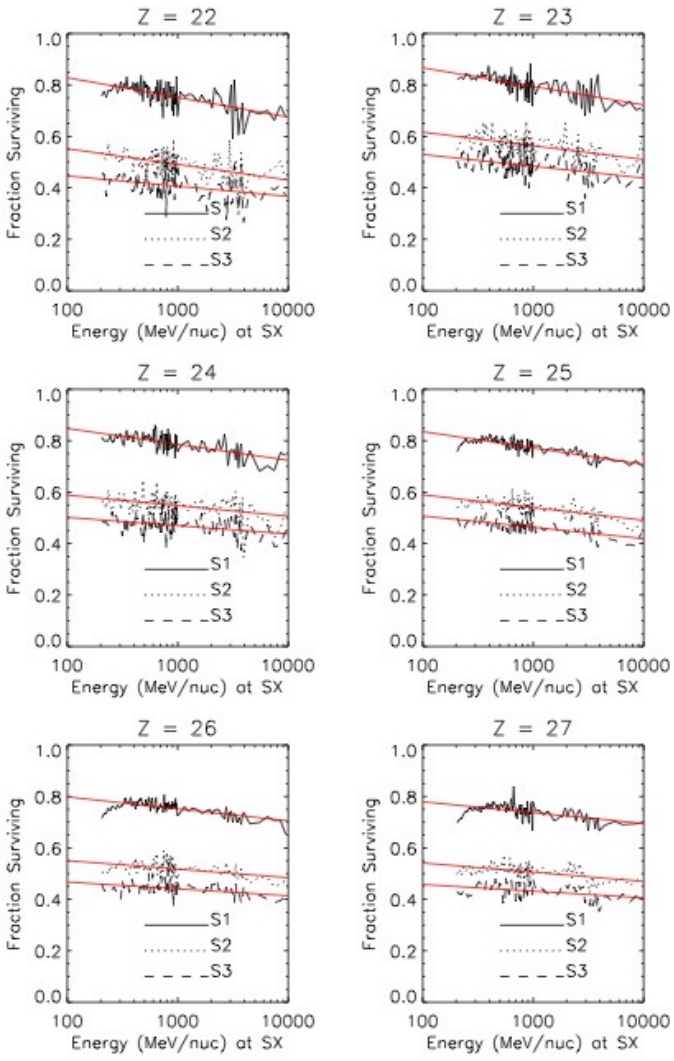

Figure 4: Particle survival fractions vs. energy for Z=22 to Z=27 from the top of the instrument through each of the scintillators, calculated by the SuperTIGER Geant4 simulation. The solid lines show survival fraction vs. energy to the top of S1, dotted lines show survival fraction vs. energy to the top of S2, and dashed lines show survival fraction vs. energy to the top of S3. The red lines show simple (linear vs. logarithmic) fits to the separate curves.

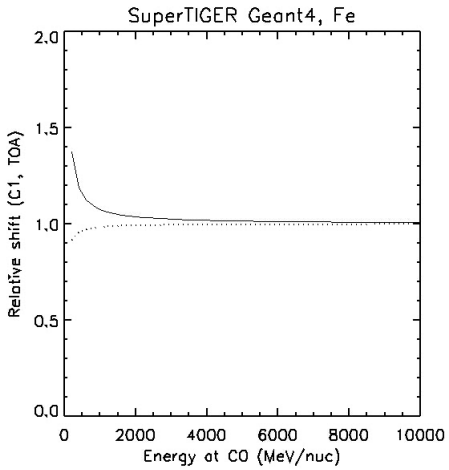

Figure 5: Geant4 calculations of $_{26}$Fe energies measured at top of atmosphere (TOA) and C1 relative to energies measured at C0.

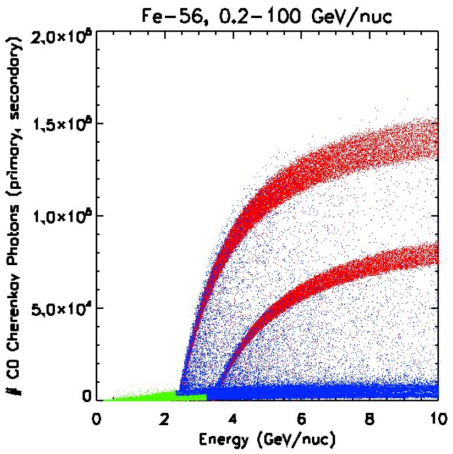

Figure 6: Geant4 simulated Aerogel Cherenkov signals due to the primary particles ($_{26}$Fe, red, for aerogel indexes n=1.043 (upper) and n=1.025 (lower)), knock-on electrons due to primary particles above threshold energy (blue), and knock-on electrons due to primary particles below threshold energy (green).

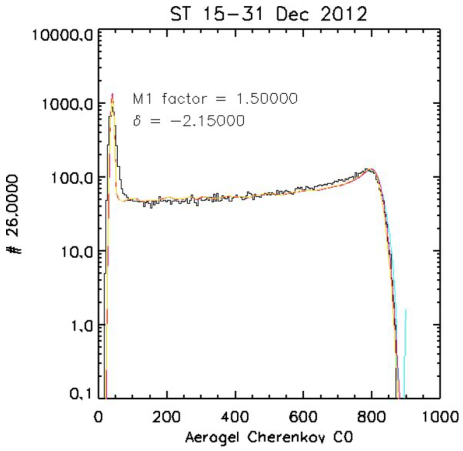

Figure 7: Fits (in color) of the flight data aerogel Cherenkov signal (black histogram) for $_{26}$Fe, assuming power law index of approximately -2.15, and ~1.5-2 pe's for Z=1, ß=1.

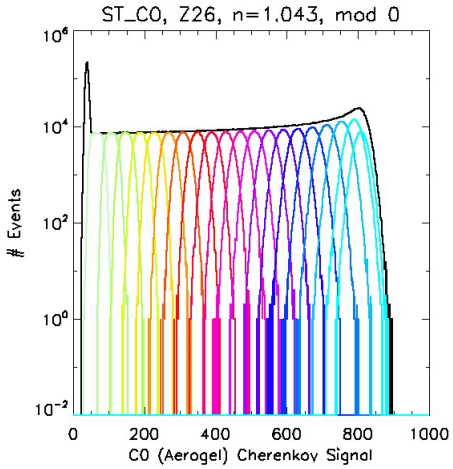

Figure 8: Aerogel Cherenkov signals for fixed energy bins, for $_{26}$Fe, n=1.043.

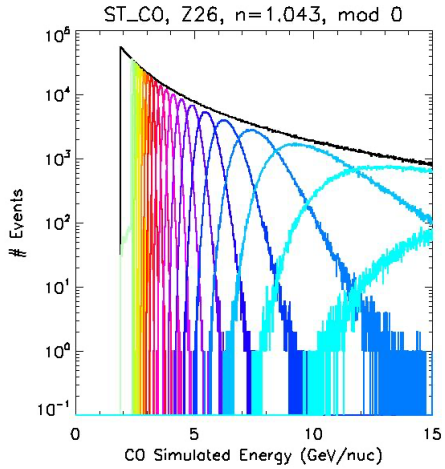

Figure 9: Energy distributions for fixed-edge Aerogel Cherenkov signals, for $_{26}$Fe, n=1.043.

6. Energy Calibration

Particle energies are obtained first by obtaining the charge Z, and assumed isotopic mass A, via particle identification from S vs C1 or C1 vs C0 data (see [1], [2], [7]), and then by obtaining velocities from the Cherenkov data.

Figure 7 shows a sample fit of the aerogel Cherenkov signal, from SuperTIGER I flight data for Fe. The soft edge at saturation (ß approaching 1) is a result of both the maximum photoelectron yield and resultant photoelectron fluctuations of the aerogel signal as well as the power-law index of the particle spectrum. The slope and curve of the "shoulder" between Cherenkov threshold (peak at left) and the saturation edge is largely due to the spectrum power law index (~2.15), and the threshold peak offset from zero is due to scintillation in plastic film in the detector, some Goretex Chernekov signal, and knock-on electrons.

Figures 8 and 9 illustrate the resulting calibration between the Cherenkov detector light yields and particle velocities, or energies per nucleon, respectively. The figures are plotted for $_{26}$Fe and for aerogel Cherenkov signals with index n=1.043. In Figure 8, particles are selected from fixed-edge energy bins (e.g. 3.0-3.1 GeV/nuc), and the corresponding aerogel Cherenkov signals are plotted as colored histograms, appearing as gaussian peaks centered on the light yields corresponding to that energy bin, smeared by photoelectron statistics and offset by background signals within the Cherenkov detector (e.g. knock-on electrons, as well as scintillation and Cherenkov light yields from materials besides the main radiator in the detector). Similarly, in Figure 9, particles are selected from fixed-edge aerogel Cherenkov bins (e.g. 290-330 in the unitless Cherenkov signal scale adopted for flight data analysis), and the corresponding energies (or GeV/nuc) are plotted as colored histograms. The resulting cross-calibration between

Cherenkov light yields and energies make possible a response matrix approach that will accommodate photoelectron statistics, knock-on electrons, and detector backgrounds, yielding calibrated energy scales for each Z in the SuperTIGER (and SuperTIGER–2) flight data sets.

Conclusion

Although work remains to be done in analyzing the simulations data, the Geant4 SuperTIGER instrument model is sufficiently complete that useful data may be generated. To date, test runs for elements from Z=10 to Z=29 have been successfully executed for millions of test particles at energies from 200 MeV/nuc to 40 GeV/nuc. Energy losses and interaction losses may now be calculated so that element abundances measured at the instrument can be corrected to the top of the instrument and top of the atmosphere.

Acknowledgements

This work was supported by NASA under grants NNX09AC17G, NNX09AC18G, NNX14AB24G, NNX14AB25G, and NNX15AC15G, by the Peggy and Steve Fossett Foundation, and by the McDonnell Center for the Space Sciences at Washington University in St. Louis.

References

[1] W.R. Binns et al, *The SuperTIGER Instrument: Measurements of Elemental Abundances of Ultra-Heavy Galactic Cosmic Rays*, The Astrophysical Journal **788** 18 (June 2014).

[2] R. Murphy et al., *Abundances of Ultra-Heavy Galactic Cosmic Rays from the SuperTIGER Instrument*, Proc. 34th International Cosmic Ray Conference, The Hague (2015).

[3] A.W. Labrador et al., *Galactic Cosmic-Ray Composition and Spectra for Ne through Cu from 0.8 to 10 GeV/nuc with the SuperTIGER Instrument*, Proc. 34th International Cosmic Ray Conference, The Hague (2015).

[4] J.J. Engelmann et al., *Charge composition and energy spectra of cosmic-ray nuclei for elements from Be to Ni. Results from HEAO-3-C2*, Astronomy and Astrophysics **233** 96 (1990).

[5] A.W. Labrador et al., *Galactic Cosmic Ray Energy Spectra for Heavy Elements (Ne to Zn) from ~0.8 to ~10 GeV/nuc with the SuperTIGER Instrument*, Proc. 36th International Cosmic Ray Conference, Madison (2019).

[6] Agostinelli, S., Allison, J., Amako, K., et al. 2003, Nuclear Instruments and Methods in Physics Research A, 506, 250. And http://geant4.web.cern.ch/

[7] N.E. Walsh et al, *SuperTIGER instrument abundances of galactic cosmic rays for the charge interval* $41 \leq Z \leq 56$, Advances in Space Research, 70, 2666 (2022).